PERGAMON Computers and Mathematics with Applications 43 (2002) 981–1002

An International Journal
computers & mathematics with applications

www.elsevier.com/locate/camwa

Three-Dimensional Infinite Elements Utilizing Basis Functions with Compact Support

A. SAFJAN AND M. NEWMAN
Department of Engineering Mechanics, University of Nebraska—Lincoln
W317-4 Nebraska Hall, P.O. Box 880526, Lincoln, NE 68588-0526, U.S.A.

(Received and accepted May 2001)

Abstract—In this paper, improvements are made in the numerical conditioning of three-dimensional infinite element stiffness matrices by replacing the characteristic (eigenfunction) basis functions which have global support with basis functions which have local support and appropriate preconditioning. The conditioning and convergence properties of these new infinite elements are presented in solving three-dimensional exterior problems for the Helmholtz equation.

Keywords—Unbounded domain problems, Infinite elements, Ill-conditioning, Helmholtz equation.

1. INTRODUCTION

In 1977, Bettess [1] suggested the idea of developing infinite elements which utilize the sequence of multipole functions

$$\left\{\frac{1}{r}, \frac{1}{r^2}, \ldots\right\}$$

as basis functions in the infinite direction r. Over the last 23 years, infinite elements utilizing various forms of these multipole basis functions have been developed and improved for one-dimensional, two-dimensional, and three-dimensional problems by Bettess *et al.* [1–10], Coyette *et al.* [11,12], Astley *et al.* [11,13–15], Burnett *et al.* [16–20], Demkowicz *et al.* [21–26], and Gerdes *et al.* [21,22,27,28] with additional contributions made by Cipolla *et al.* [29], Harari *et al.* [30,31], and Shirron *et al.* [32,33]. From the computational point of view, a very successful multipole-based infinite element for solving three-dimensional exterior wave problems has been developed by Burnett [16,17]. In this paper, we will build on the ideas of those referenced above in using infinite elements to solve three-dimensional exterior wave problems.

Consider the following three-dimensional problem for the Helmholtz equation:

$$\begin{aligned} -\Delta u - k^2 u &= 0, \qquad \text{in } \Omega, \\ \left.\frac{\partial u}{\partial n}\right|_{\partial\Omega} &= g, \qquad \lim_{r\to\infty} r\left(\frac{\partial u}{\partial r} + iku\right) = 0, \end{aligned} \tag{1}$$

Support of this work by the Office of Naval Research (ONR) under the Grant #N00014-99-1-0778 is gratefully acknowledged.

0898-1221/02/$ - see front matter Typeset by $\mathcal{A}\mathcal{M}\mathcal{S}$-TEX
PII: S0898-1221(01)00340-6

where $\Omega \subset \mathbb{R}^3$ is the region

$$\Omega = \{(r, \theta, \phi) \mid r > r_1,\ 0 \leq \theta \leq \pi,\ 0 \leq \phi < 2\pi\}$$

outside the sphere $\partial\Omega$

$$\partial\Omega = \{(r_1, \theta, \phi) \mid 0 \leq \theta \leq \pi,\ 0 \leq \phi < 2\pi\}$$

of radius r_1, $\frac{\partial u}{\partial n}|_{\partial\Omega}$ denotes the normal derivative of u on $\partial\Omega$, and (r, θ, ϕ) are the usual spherical coordinates.

A methodology for constructing the infinite elements used to solve exterior problems for the Helmholtz equation is to base the infinite elements on convergent series expansions. This has been done by, e.g., Burnett [16–20], who developed infinite elements based on the multipole expansion

$$u\left(\rho, \hat{\theta}, \hat{\phi}\right) = \sum_{n=1}^{\infty} \frac{G_n\left(\hat{\theta}, \hat{\phi}\right)}{\rho^n} e^{-ik\rho}$$

in prolate and oblate spheroidal coordinates $(\rho, \hat{\theta}, \hat{\phi})$, where ρ is the spheroidal radius, $\hat{\theta}$ is the spheroidal elevation angle, and $\hat{\phi}$ is the azimuthal angle. This spheroidal multipole expansion investigated by Holford [34] is the generalization in prolate and oblate spheroidal coordinates of the classical multipole expansion of Atkinson and Wilcox [34–37]

$$u(r, \theta, \phi) = \sum_{n=1}^{\infty} \frac{G_n(\theta, \phi)}{r^n} e^{-ikr}$$

in spherical coordinates. To develop an infinite element based on the spheroidal multipole expansion, we define basis functions $\varphi^j(\rho, \hat{\theta}, \hat{\phi})$ by taking the tensor product of the functions

$$\frac{e^{-ik\rho}}{\rho^n}, \qquad \text{for } n = 1, 2, \ldots, \tag{2}$$

in the radial direction with Lagrange polynomial shape functions in the angular directions. The corresponding approximate solution is

$$u_h\left(\rho, \hat{\theta}, \hat{\phi}\right) = \sum_j u_j \varphi^j\left(\rho, \hat{\theta}, \hat{\phi}\right). \tag{3}$$

Now there exists a serious computational problem with this multipole infinite element, namely, numerical ill-conditioning [26,32,33]. To illustrate this, an attempt was made to solve the exterior wave problem (1) with $r_1 = 11$, $k = 1$, and $g = -kh'^{(2)}_{10}(kr_1)P_{10}(\cos\theta)$ using a mesh of 100 multipole infinite elements with the functions (2) in the radial direction and fifth-order Lagrange polynomial shape functions in the angular directions. The results of this endeavor are given in Figure 1. Figure 1 is a graph of the normalized error $\|u - u_h\|_{H^1_w(\Omega)} / \|u\|_{H^1_w(\Omega)}$ between the exact and approximate solutions u and u_h, respectively, and the stiffness matrix condition number versus the number of multipole terms.

From Figure 1 it is seen that the multipole infinite elements give an exponential rate of convergence until the number of multipole terms reaches 10. When the number of multipole terms exceeds 10, the error stops its downward trend and oscillates in the range from 10^{-3} to 10^{-4}. The reason for this behavior is that the condition number of the stiffness matrix is above the order 10^{16} which is the limit of the arithmetic precision of a typical workstation.

Consequently, in order to improve the numerical conditioning, we consider replacing the radial functions (2) with functions having localized support. Similar to the usual finite element formulation, we create a "piecewise" multipole infinite element where the localized radial functions

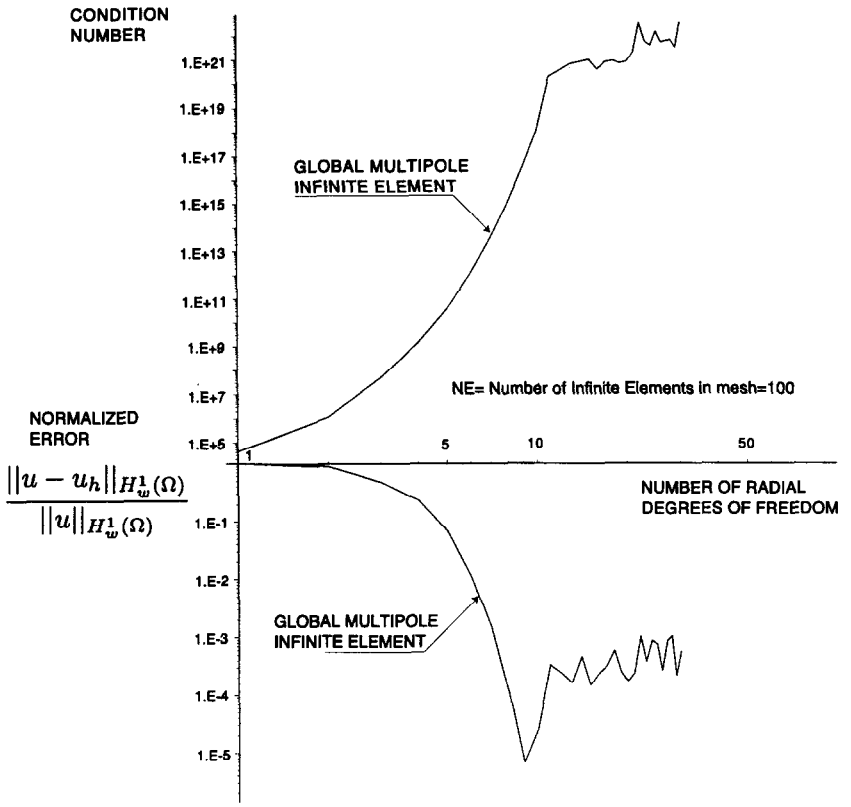

Figure 1. Ill-conditioning of the spherical multipole infinite element.

are Lagrange interpolation polynomials in the variable $1/\rho$. By utilizing radial functions with localized support, the stiffness matrix of the piecewise multipole infinite element is more sparsely populated and may have better numerical conditioning for the same number of degrees of freedom than the stiffness matrix of the usual multipole infinite element.

In this paper, we will develop infinite elements based on the spheroidal multipole expansion of the solution to the three-dimensional Helmholtz equation and the Sommerfeld radiation condition. The infinite elements to be developed will utilize compact support basis functions that are localized versions of the global functions appearing in the multipole expansion. By using compact support basis functions, the numerical ill-conditioning grows at a slower rate and allows a better approximation accuracy to be obtained as compared with the basis functions that have global support.

2. SPHEROIDAL MULTIPOLE EXPANSIONS

In order to introduce the spherical and spheroidal multipole expansion theorems, we must first consider the following definitions [36].

DEFINITION. *An exterior region $\Omega \subset \mathbb{R}^3$ is a region (open connected set) consisting of all points outside a closed bounded surface $\partial\Omega \subset \mathbb{R}^3$.*

DEFINITION. *A radiation function for the exterior region $\Omega \subset \mathbb{R}^3$ is a complex-valued function $u(\mathbf{x})$ which satisfies:*

(1) *$u(\mathbf{x})$ is of class C^2 and satisfies the Helmholtz equation*

$$-\Delta u(\mathbf{x}) - k^2 u(\mathbf{x}) = 0$$

in the closure of Ω, and

(2) $u(\mathbf{x})$ *satisfies Sommerfeld's radiation condition,*

$$\lim_{R\to\infty}\int_{r=R}\left|\frac{\partial u}{\partial r}(\mathbf{x})+iku(\mathbf{x})\right|^2 ds=0,$$

where $k>0$.

Here $\mathbf{x}\in\mathbb{R}^3$ is the position vector

$$\mathbf{x}=r\sin\theta(\cos\phi\mathbf{i}+\sin\phi\mathbf{j})+r\cos\theta\mathbf{k}$$

in spherical coordinates

$$r\geq 0,\qquad 0\leq\theta\leq\pi,\qquad 0\leq\phi<2\pi.$$

The eigenfunction representation of a radiation function $u(\mathbf{x})$ is given by

$$u(r,\theta,\phi)=\sum_{n=0}^{\infty}\sum_{m=0}^{n}c_{nm}h_n^{(2)}(kr)P_n^m(\cos\theta)e^{im\phi}, \tag{4}$$

where $h_n^{(2)}(x)$ are the spherical Hankel functions of the second kind and $P_n^m(x)$ are the associated Legendre functions of the first kind. We recall [38] that the spherical Hankel functions of the second kind are given by

$$h_n^{(2)}(x)=\frac{i}{x}p_n\left(\frac{1}{x}\right)e^{-ix},\qquad \text{for } n=0,1,2,\ldots, \tag{5}$$

where p_n are polynomials defined by the recurrence relation

$$p_{n+1}(x)=(2n+1)xp_n(x)-p_{n-1}(x),\qquad \text{for } n=1,2,\ldots, \tag{6}$$

and

$$p_0(x)=1,\qquad p_1(x)=x+i. \tag{7}$$

Now the eigenfunction expansion of the radiation function (4) and the expansion of the spherical Hankel functions (5) suggest the classical multipole expansion theorem due to Atkinson and Wilcox [34–37].

EXPANSION THEOREM. *Let* $u(\mathbf{x})$ *be a radiation function for the region exterior to a sphere* $|\mathbf{x}-\mathbf{x}_0|=c$, *and let* (r,θ,ϕ) *be the spherical coordinates for* $\mathbf{x}$ *relative to an origin at* $\mathbf{x}_0$. *Then*

$$u(r,\theta,\phi)=e^{-ikr}\sum_{n=1}^{\infty}\frac{G_n(\theta,\phi)}{r^n}, \tag{8}$$

where the series converges for $r>c$ *and converges absolutely and uniformly in* r, θ, *and* ϕ *in any region* $r\geq c+\epsilon>c$. *The series may be differentiated term by term with respect to* r, θ, *and* ϕ *any number of times, and the resulting series all converge absolutely and uniformly.*

Now in [34], Holford extended this multipole expansion theorem of Atkinson and Wilcox to

$$u\left(\rho,\hat{\theta},\hat{\phi}\right)=e^{-ik\rho}\sum_{n=1}^{\infty}\frac{G_n\left(\hat{\theta},\hat{\phi}\right)}{\rho^n} \tag{9}$$

in *prolate spheroidal* coordinates

$$\mathbf{x}=\sqrt{\rho^2-f^2}\sin\hat{\theta}\left(\cos\hat{\phi}\mathbf{i}+\sin\hat{\phi}\mathbf{j}\right)+\rho\cos\hat{\theta}\mathbf{k}$$

and *oblate spheroidal* coordinates

$$\mathbf{x}=\rho\sin\hat{\theta}\left(\cos\hat{\phi}\mathbf{i}+\sin\hat{\phi}\mathbf{j}\right)+\sqrt{\rho^2-f^2}\cos\hat{\theta}\mathbf{k},$$

where

$$f\geq 0,\qquad \rho\geq f,\qquad 0\leq\hat{\theta}\leq\pi,\qquad 0\leq\hat{\phi}<2\pi.$$

3. PIECEWISE MULTIPOLE INFINITE ELEMENTS

Model Problem

We now consider the exterior wave problem (1) with the domain taken to be the region

$$\Omega = \left\{ \left(\rho, \hat{\theta}, \hat{\phi} \right) \mid \rho > \rho_1,\ 0 \le \hat{\theta} \le \pi,\ 0 \le \hat{\phi} < 2\pi \right\}$$

outside the prolate spheroid

$$\partial\Omega = \left\{ \left(\rho_1, \hat{\theta}, \hat{\phi} \right) \mid 0 \le \hat{\theta} \le \pi,\ 0 \le \hat{\phi} < 2\pi \right\}$$

of spheroidal radius ρ_1.

A weighted and conjugated weak form of (1) is [21–28]

$$a(u, v) = l(v), \qquad \forall\, v \in \mathcal{V}, \quad u \in \mathcal{V}, \tag{10}$$

where

$$a(u, v) = \int_0^{\pi} \int_0^{2\pi} \int_{\rho_1}^{\infty} \frac{1}{\rho^2} \left(\nabla u \cdot \nabla \bar{v} - k^2 u \bar{v} - \frac{2}{\rho} g^{\rho\rho} \frac{\partial u}{\partial \rho} \bar{v} \right) J \, d\rho \, d\hat{\phi} \, d\hat{\theta} \tag{11}$$

is the sesquilinear form,

$$l(v) = \int_{\partial\Omega} \frac{1}{\rho^2} g \bar{v} \, ds \tag{12}$$

is the antilinear functional, and $\mathcal{V} = H^1_w(\Omega)$. Here $H^1_w(\Omega)$ is the complex weighted Sobolev space endowed with the norm

$$\|u\|_{H^1_w(\Omega)} = \sqrt{\int_0^{\pi} \int_0^{2\pi} \int_{\rho_1}^{\infty} \frac{1}{\rho^2} \left(|\nabla u|^2 + |u|^2 \right) J \, d\rho \, d\hat{\phi} \, d\hat{\theta}}. \tag{13}$$

For prolate spheroidal coordinates

$$g^{\rho\rho} = \frac{\rho^2 - f^2}{\rho^2 - (f^2/2)\left(1 + \cos 2\hat{\theta}\right)},$$

$$J = \left(\rho^2 - \frac{f^2}{2} \left(1 + \cos 2\hat{\theta} \right) \right) \sin \hat{\theta} > 0.$$

It should be emphasized that the Sommerfeld radiation condition given in (1) is not incorporated into the definition of the function space $\mathcal{V}$, and therefore must be incorporated by some other means (see, e.g., [21]). This is not necessary when formulating the approximate problem since only the basis functions satisfying the Sommerfeld condition are used.

The function g in (1) is chosen so that the exact solution reads

$$u\left(\rho, \hat{\theta}, \hat{\phi}\right) = h_1^{(2)}\left(kr\left(\rho, \hat{\theta}, \hat{\phi}\right)\right) P_1\left(\cos\theta\left(\rho, \hat{\theta}, \hat{\phi}\right)\right),$$

where the transformation from prolate spheroidal to spherical coordinates is given by

$$r = \sqrt{\rho^2 - \frac{f^2}{2}\left(1 - \cos 2\hat{\theta}\right)}, \quad \cos\theta = \frac{\rho \cos\hat{\theta}}{\sqrt{\rho^2 - (f^2/2)\left(1 - \cos 2\hat{\theta}\right)}}, \qquad \phi = \hat{\phi}.$$

In the convergence study to be presented, we are interested in investigating the behavior of the approximate solution u_h arising from the piecewise multipole infinite element formulation on the boundary $\partial\Omega$ and comparing this behavior to that of the global multipole infinite element. In order to investigate this behavior on the boundary $\partial\Omega$, we consider the function space $L^2(\partial\Omega)$ endowed with the norm

$$\|u\|_{L^2(\partial\Omega)} = \sqrt{\int_{\partial\Omega} |u|^2 \, ds}. \tag{14}$$

Piecewise Infinite Element Based on the Spheroidal Multipole Expansion

We now introduce a three-dimensional piecewise infinite element based on the spheroidal multipole expansion given in (9). First, letting

$$\begin{aligned} n_e &= \text{number of radial subintervals in the mesh,} \\ n &= \text{number of nodes per radial subinterval,} \\ n_n &= \text{total number of radial nodes in the mesh,} \end{aligned}$$

the radial interval $[\rho_1, \infty)$ is partitioned into n_e subintervals where each of the radial subintervals $e_r = 1, \ldots, n_e - 1$ is bounded, while the radial subinterval $e_r = n_e$ is unbounded. Each radial subinterval has n local nodes and corresponding n Lagrange polynomials in the variable $1/\rho$. The number of radial nodes for this partitioning is

$$n_n = (n-1)n_e.$$

Next, letting

$$\begin{aligned} m_e &= \text{number of two-dimensional angular subdomains in the mesh,} \\ m &= \text{number of nodes per angular subdomain,} \\ m_n &= \text{total number of angular nodes in the mesh,} \end{aligned}$$

the two-dimensional angular region $[0, \pi] \times [0, 2\pi)$ is partitioned into m_e subdomains, and each of the angular subdomains $e_a = 1, \ldots, m_e$ has m local nodes. This partitioning of the radial and angular domains results in the Cartesian product partitioning of the domain Ω into $n_e \times m_e$ subdomains ${}^{(e_r,e_a)}\Omega$. The number of global nodes for the infinite element mesh is $n_n \times m_n$.

In the radial coordinate the shape functions, for $e_r = 1, \ldots, n_e - 1$, are

$$\sigma_\kappa(\rho) = \frac{\prod\limits_{\substack{\lambda=1 \\ \lambda \neq \kappa}}^{n} (1/\rho - 1/\rho_\lambda)}{\prod\limits_{\substack{\lambda=1 \\ \lambda \neq \kappa}}^{n} (1/\rho_\kappa - 1/\rho_\lambda)} e^{-ik\rho}, \qquad \text{for } \kappa = 1, 2, \ldots, n, \tag{15}$$

where $\rho_1, \rho_2, \ldots, \rho_n$ are the nodal coordinates. To perform integrations in the radial direction, we introduce the transformation ${}^{(e_r)}T\colon [-1, 1] \to [\rho_1, \rho_n]$

$${}^{(e_r)}T(\zeta) = \frac{1}{(1/2)(1/\rho_n - 1/\rho_1)\zeta + (1/2)(1/\rho_n + 1/\rho_1)}, \tag{16}$$

with Jacobian

$${}^{(e_r)}J(\zeta) = -\frac{(1/2)(1/\rho_n - 1/\rho_1)}{\left((1/2)(1/\rho_n - 1/\rho_1)\zeta + (1/2)(1/\rho_n + 1/\rho_1)\right)^2}. \tag{17}$$

Therefore, for $e_r = 1, \ldots, n_e - 1$, the integrals in the radial direction are transformed as

$$\int_{\rho_1}^{\rho_n} f(\rho)\, d\rho = \int_{-1}^{1} f\left({}^{(e_r)}T(\zeta)\right) {}^{(e_r)}J(\zeta)\, d\zeta.$$

For $e_r = n_e$, we take the limit as $\rho_n \to \infty$. Consequently, the shape functions become

$$\sigma_\kappa(\rho) = \frac{(1/\rho)\prod\limits_{\substack{\lambda=1 \\ \lambda \neq \kappa}}^{n-1} (1/\rho - 1/\rho_\lambda)}{(1/\rho_\kappa)\prod\limits_{\substack{\lambda=1 \\ \lambda \neq \kappa}}^{n-1} (1/\rho_\kappa - 1/\rho_\lambda)} e^{-ik\rho}, \qquad \text{for } \kappa = 1, 2, \ldots, n-1. \tag{18}$$

The transformation ${}^{(e_r)}T : [-1,1) \to [\rho_1, \infty)$ and the Jacobian read, respectively,

$$ {}^{(e_r)}T(\zeta) = \frac{2\rho_1}{1-\zeta}, \tag{19} $$

$$ {}^{(e_r)}J(\zeta) = \frac{2\rho_1}{(1-\zeta)^2}. \tag{20} $$

Thus, for $e_r = n_e$, the integrals in the radial direction are transformed as

$$ \int_{\rho_1}^{\infty} f(\rho)\, d\rho = \int_{-1}^{1} f\left({}^{(e_r)}T(\zeta)\right) {}^{(e_r)}J(\zeta)\, d\zeta. $$

This meshing of the unbounded radial domain is illustrated in Figure 2.

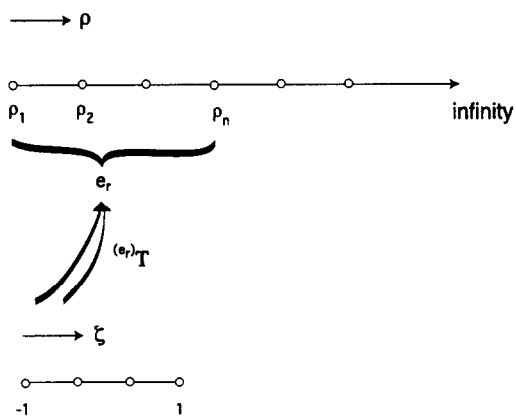

Figure 2. 1-D meshing of the unbounded radial domain.

In the angular coordinates, we introduce standard Lagrange interpolation functions $\chi_i(\xi,\eta)$ on the unit square $[-1,1] \times [-1,1]$ where the transformation from local coordinates (ξ,η) to global angular coordinates $(\hat{\theta},\hat{\phi})$ is given by

$$ \hat{\theta}(\xi,\eta) = \sum_i \hat{\theta}_i \chi_i(\xi,\eta), \qquad \hat{\phi}(\xi,\eta) = \sum_i \hat{\phi}_i \chi_i(\xi,\eta) \tag{21} $$

and the global angular shape functions are given by

$$ \hat{\chi}_i\left(\hat{\theta},\hat{\phi}\right) = \chi_i\left(\xi\left(\hat{\theta},\hat{\phi}\right), \eta\left(\hat{\theta},\hat{\phi}\right)\right). \tag{22} $$

Taking the tensor product of the radial shape functions with the angular shape functions gives the infinite element shape functions $\varphi_j(\rho,\xi,\eta)$.

Now the integrals involved in the computation of the infinite element stiffness matrices can be separated in the radial and angular variables in the following sense:

$$ \int_{\rho_1}^{\infty}\int_{-1}^{1}\int_{-1}^{1} f(\rho)g(\xi,\eta)\, d\xi\, d\eta\, d\rho = \left(\int_{\rho_1}^{\infty} f(\rho)\, d\rho\right)\left(\int_{-1}^{1}\int_{-1}^{1} g(\xi,\eta)\, d\xi\, d\eta\right). $$

This separability greatly reduces the computational effort involved in generating the local stiffness matrices. Taking advantage of the separability of the radial and angular variables, we introduce the approximate solution and test functions

$$ u_h(\rho,\xi,\eta) = \sum_{\lambda=1}^{n_n}\sum_{\nu=1}^{m_n} u_{(\lambda-1)m_n+\nu}\sigma_\lambda(\rho)\chi_\nu(\xi,\eta), \qquad v_h(\rho,\xi,\eta) = \sigma_\kappa(\rho)\chi_\mu(\xi,\eta) $$

into the weak form (10)–(12) which yields the system of linear equations

$$ \sum_{\lambda=1}^{n_n}\sum_{\nu=1}^{m_n}\left(R_1^{\kappa\lambda}A_3^{\mu\nu} + R_2^{\kappa\lambda}A_2^{\mu\nu} + R_3^{\kappa\lambda}A_1^{\mu\nu}\right) u_{(\lambda-1)m_n+\nu} = V^{\kappa}W^{\mu}, \tag{23} $$

for $\kappa = 1,2,\ldots,n_n$ and $\mu = 1,2,\ldots,m_n$. Here $R_1^{\kappa\lambda}$, $R_2^{\kappa\lambda}$, $R_3^{\kappa\lambda}$, V^{κ} are matrices involving only radial integrations and $A_1^{\mu\nu}$, $A_1^{\mu\nu}$, $A_1^{\mu\nu}$, W^{μ} are matrices involving only angular integrations.

Convergence Study of the Piecewise Multipole Infinite Element

The piecewise multipole infinite element was applied to solve the exterior wave problem (1) with $k = 1$. In this convergence study, we consider two prolate spheroidal boundaries $\partial\Omega$ of radius $\rho_1 = 11$ and having aspect ratios of 3:1 and 7:1 which corresponds to $f = 22\sqrt{2}/3$ and $f = 44\sqrt{3}/7$, respectively.

The distribution of the radial nodes for this infinite element is based on the transformation ${}^{\infty}T\colon [1,0) \to [\rho_1, \infty)$

$$ {}^{\infty}T(z) = \frac{\rho_1}{z}. $$

We will consider two distributions of the radial nodes. The first is based on a uniform partition of the interval $[1,0)$ into n_n subintervals which yields the radial coordinate distribution

$$ \rho_\kappa = {}^{\infty}T\left(1 + \frac{1-\kappa}{n_n}\right), \qquad \text{for } \kappa = 1, 2, \ldots, n_n. \tag{24} $$

The second is a nonuniform partition of the interval $[1,0)$ into n_n subintervals which yields the radial coordinate distribution

$$ \rho_\kappa = {}^{\infty}T\left(1 + \frac{\kappa(1-\kappa)}{n_n(n_n+1)}\right), \qquad \text{for } \kappa = 1, 2, \ldots, n_n. \tag{25} $$

In this convergence study, the normalized error

$$ e_\Omega = \frac{\|u - u_h\|_{H^1_w(\Omega)}}{\|u\|_{H^1_w(\Omega)}} $$

on Ω is measured via the norm given in (13) and the normalized boundary error

$$ e_{\partial\Omega} = \frac{\|u - u_h\|_{L^2(\partial\Omega)}}{\|u\|_{L^2(\partial\Omega)}} $$

on $\partial\Omega$ is measured via the norm given in (14).

The infinite element meshes corresponding to the prolate spheroidal boundaries are illustrated in Figures 3 and 6. The convergence results given in Figures 4, 5, 7–10 compare the performance of the piecewise multipole infinite elements with the global multipole infinite element introduced in Section 1. Each infinite element utilizes fifth-order Lagrange polynomial shape functions in the angular variable θ, and each piecewise infinite element utilizes p^{th}-order Lagrange polynomial shape functions in the variable $1/\rho$. The infinite element meshes considered in this convergence study consist of 100 infinite elements. Thus, in this convergence study we introduce a high level of approximation in the angular directions in order to isolate the convergence properties as the approximation is enriched in the radial direction only. All computations in this convergence study were done using standard 16-digit precision arithmetics.

Figures 4, 7, and 9 show the normalized boundary error $e_{\partial\Omega}$ graphed against the number of radial degrees of freedom in logarithmic coordinates for the aspect ratios of 3:1 and 7:1, respectively. It is observed that the global multipole element gives an exponential rate of convergence on the boundary $\partial\Omega$ until the number of multipole terms reaches 10. When the number of multipole terms exceeds 10, a divergent behavior begins to occur apparently due to ill-conditioning. Each p^{th}-order piecewise multipole element also gives convergence, and each convergence curve appears to be linear. For the 3:1 aspect ratio, the minimum boundary error achieved by the global multipole element is $e_{\partial\Omega} \approx 7 \times 10^{-4}$, while the minimum boundary error achieved by the piecewise multipole elements is $e_{\partial\Omega} \approx 1 \times 10^{-7}$ with the uniform radial mesh. For the 7:1 aspect ratio, the minimum boundary error achieved by the global multipole element is $e_{\partial\Omega} \approx 5 \times 10^{-2}$.

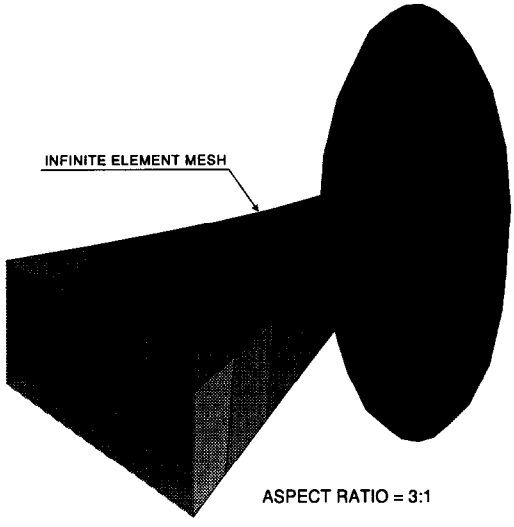

Figure 3. Prolate piecewise multipole infinite element mesh. Aspect ratio = 3:1.

NORMALIZED BOUNDARY ERROR

$$e_{\partial\Omega} = \frac{||u - u_h||_{L^2(\partial\Omega)}}{||u||_{L^2(\partial\Omega)}}$$

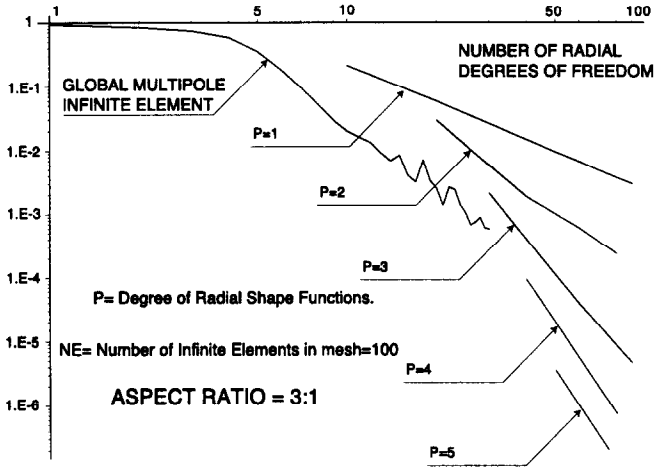

Figure 4. Comparison of the boundary convergence curves of the global multipole and piecewise multipole infinite elements. Weighted and conjugated formulation. Aspect ratio = 3:1. Uniform radial mesh.

The minimum boundary error achieved by the piecewise multipole elements is $e_{\partial\Omega} \approx 2 \times 10^{-3}$ with the uniform radial mesh and $e_{\partial\Omega} \approx 1 \times 10^{-7}$ with the nonuniform radial mesh.

Figures 5, 8, and 10 show the normalized error e_Ω and stiffness matrix condition number graphed against the number of radial degrees of freedom in logarithmic coordinates for the aspect ratios of 3:1 and 7:1, respectively. It is observed that the global multipole element gives an exponential rate of convergence on the domain Ω until the level of numerical ill-conditioning destroys the accuracy. It is observed that each p^{th}-order piecewise infinite element gives convergence in the radial direction, and each convergence curve appears to be linear. In Figure 5, where the aspect ratio is 3:1 and the radial mesh is uniform, it is observed that each piecewise convergence curve has slope approximately equal to p. The same is true in Figure 7 where the

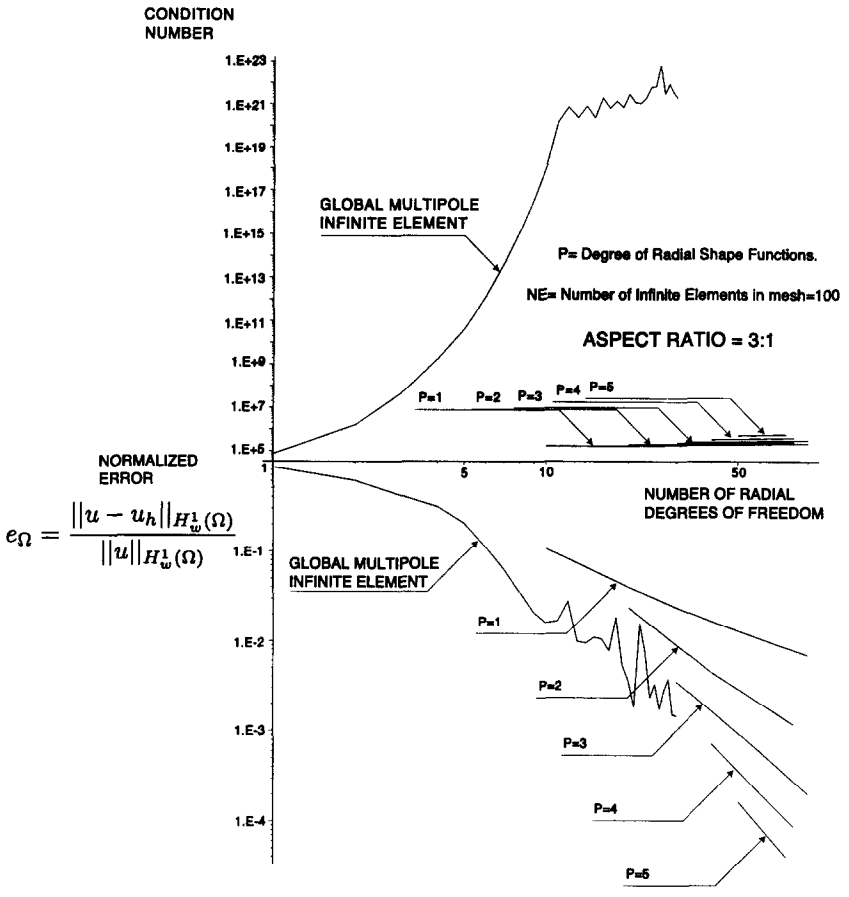

Figure 5. Comparison of the assembled stiffness matrix condition numbers and domain convergence curves of the global multipole and piecewise multipole infinite elements. Weighted and conjugated formulation. Aspect ratio = 3:1. Uniform radial mesh.

aspect ratio is 7:1 and the radial mesh is nonuniform. However, in Figure 6 where the aspect ratio is 7:1 and the radial mesh is uniform, the slopes of piecewise convergence curves appear to be equal, which suggests that the asymptotic range has not been reached. It is observed that the condition number of each p^{th}-order piecewise infinite element stiffness matrix grows linearly and the slopes of these curves are all equal. The value of the largest piecewise infinite element condition number is observed to be of the order 10^7.

Comparing the performance of the piecewise multipole infinite element with the global multipole infinite element discussed in the introductory section, we see that the piecewise multipole element competes with the global multipole element in terms of convergence rate and yields better approximation accuracy when $p = 3, 4, 5$. Also, we see that the condition number of the global multipole element grows at an exponential rate compared to the linear rate of the piecewise multipole element for $p = 1, 2, 3, 4, 5$. Thus, we see that by replacing the radial functions having global support with radial functions that have local support, the ill-conditioning grows at a slower rate which allows a better approximation accuracy to be obtained and facilitates the use of iterative linear equation solvers.

4. UNWEIGHTED AND UNCONJUGATED WEAK FORMULATION

In Section 3, the piecewise multipole infinite element was applied to solve model problem (1) using the weighted and conjugated (WC) weak formulation given in (10)–(12). We now consider

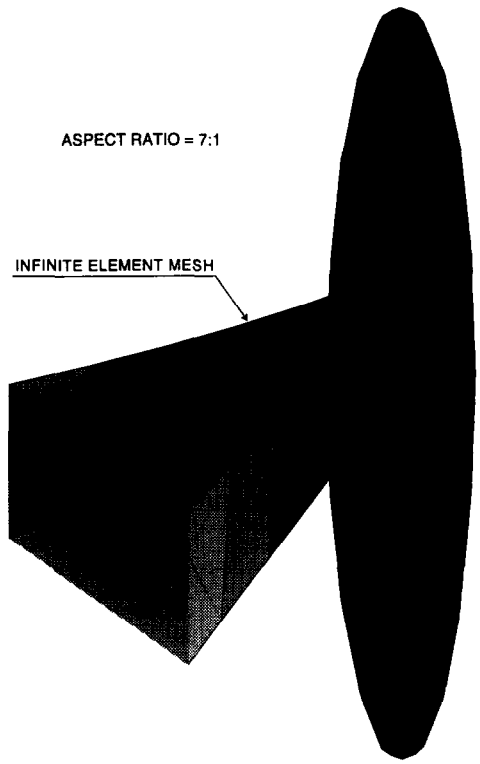

Figure 6. Prolate piecewise multipole infinite element mesh. Aspect ratio = 7:1.

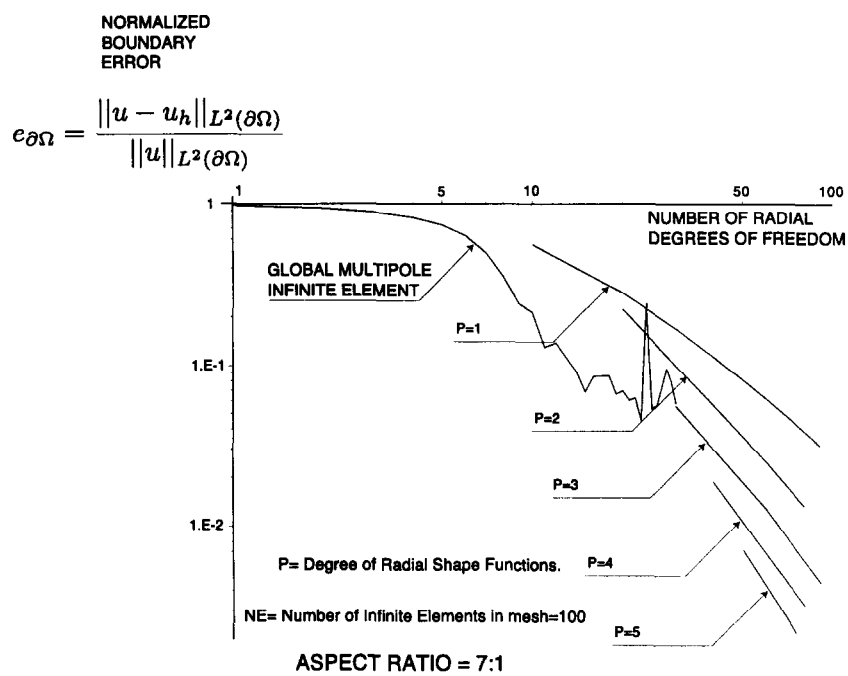

Figure 7. Comparison of the boundary convergence curves of the global multipole and piecewise multipole infinite elements. Weighted and conjugated formulation. Aspect ratio = 7:1. Uniform radial mesh.

an implementation of this infinite element using an unweighted and unconjugated (UWUC) weak formulation of model problem (1). For more details on the various weak formulations of the exterior wave problem for the Helmholtz equation, see [21–28].

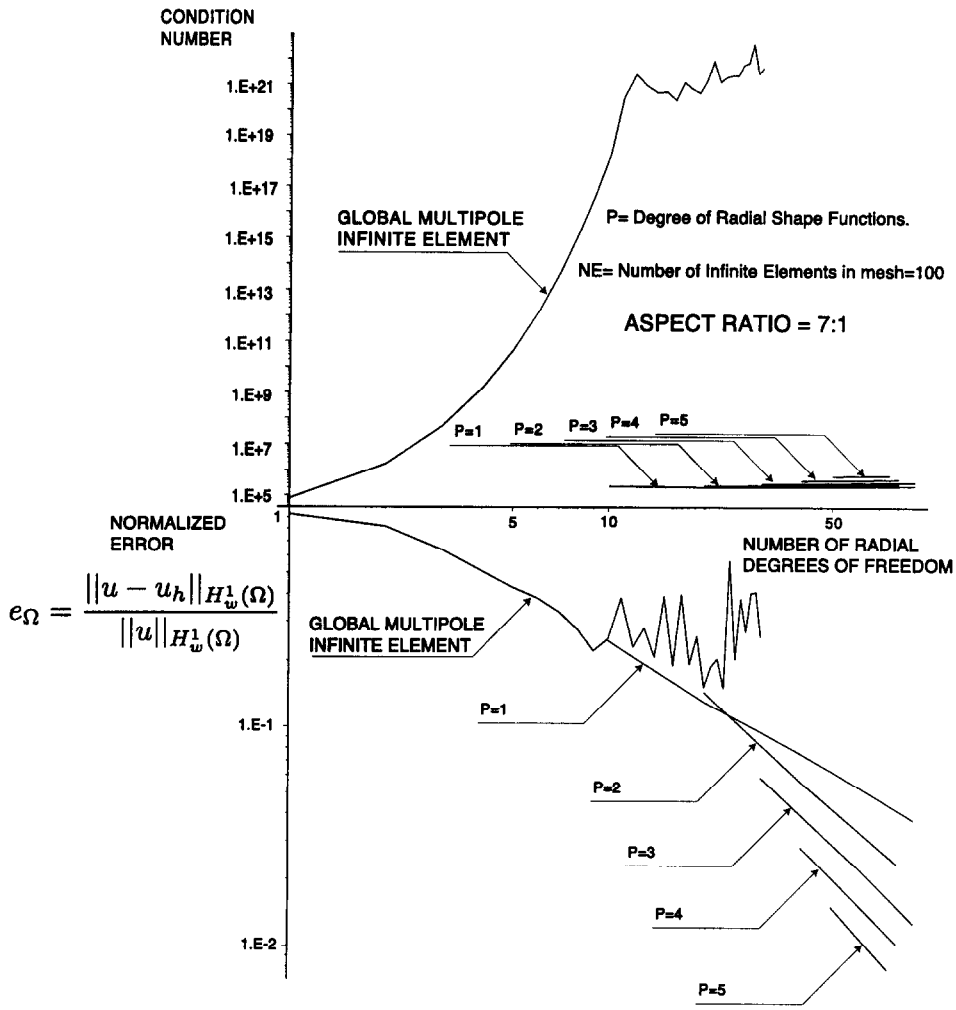

Figure 8. Comparison of the assembled stiffness matrix condition numbers and domain convergence curves of the global multipole and piecewise multipole infinite elements. Weighted and conjugated formulation. Aspect ratio = 7:1. Uniform radial mesh.

Model Problem

Once again, we consider the exterior wave problem (1) with the region

$$\Omega = \left\{ \left(\rho, \hat{\theta}, \hat{\phi} \right) \mid \rho > \rho_1,\ 0 \le \hat{\theta} \le \pi,\ 0 \le \hat{\phi} < 2\pi \right\}$$

outside the prolate spheroid

$$\partial\Omega = \left\{ \left(\rho_1, \hat{\theta}, \hat{\phi} \right) \mid 0 \le \hat{\theta} \le \pi,\ 0 \le \hat{\phi} < 2\pi \right\}$$

of radius ρ_1.

The unweighted and unconjugated weak form of the exterior wave problem (1) is

$$a(u,v) = l(v), \qquad \forall\, v \in \mathcal{V}, \quad u \in \mathcal{V}, \tag{26}$$

where

$$\begin{aligned} a(u,v) = & \lim_{\rho\to\infty} \int_0^{\pi} \int_0^{2\pi} \int_{\rho_1}^{\rho} \left(\nabla u \cdot \nabla v - k^2 uv \right) J \, d\rho \, d\hat{\phi} \, d\hat{\theta} \\ & - \lim_{\rho\to\infty} \left(\rho^2 - f^2 \right) \int_0^{\pi} \int_0^{2\pi} \frac{\partial u}{\partial \rho} v \sin\hat{\theta} \, d\hat{\phi} \, d\hat{\theta} \end{aligned} \tag{27}$$

NORMALIZED
BOUNDARY
ERROR

$$e_{\partial\Omega} = \frac{||u - u_h||_{L^2(\partial\Omega)}}{||u||_{L^2(\partial\Omega)}}$$

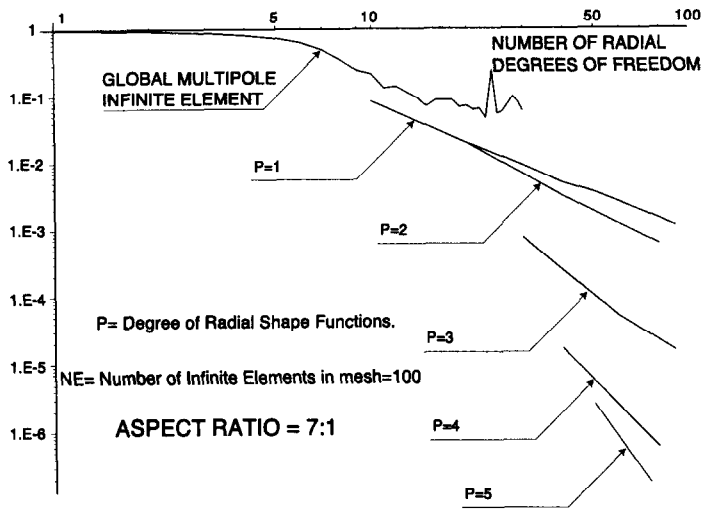

Figure 9. Comparison of the boundary convergence curves of the global multipole and piecewise multipole infinite elements. Weighted and conjugated formulation. Aspect ratio = 7:1. Nonuniform radial mesh.

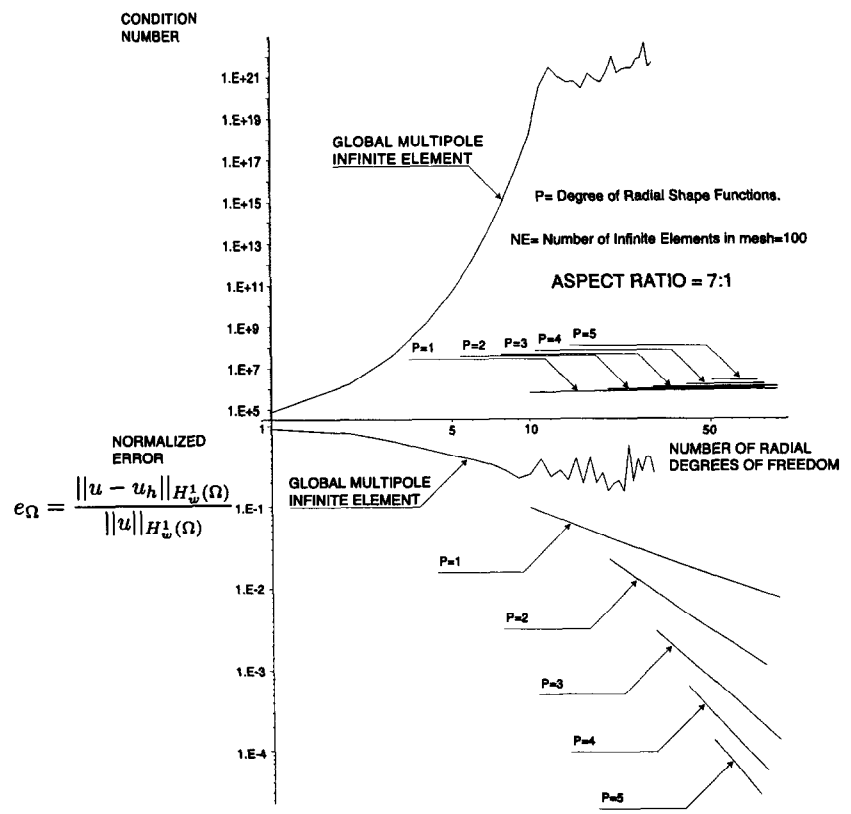

Figure 10. Comparison of the assembled stiffness matrix condition numbers and domain convergence curves of the global multipole and piecewise multipole infinite elements. Weighted and conjugated formulation. Aspect ratio = 7:1. Nonuniform radial mesh.

is the bilinear form,

$$l(v) = \int_{\partial\Omega} gv\, ds \tag{28}$$

is the linear functional, and $\mathcal{V} = H^1_w(\Omega)$. Here $H^1_w(\Omega)$ is the complex weighted Sobolev space endowed with the norm given in (13). For prolate spheroidal coordinates,

$$J = \left(\rho^2 - \frac{f^2}{2}\left(1 + \cos 2\hat{\theta}\right)\right)\sin\hat{\theta} > 0.$$

We emphasize that the radial integration given in (27) is understood in the Cauchy principal value (CPV) sense, and the Sommerfeld radiation condition given in (1) is not incorporated into the definition of the function space $\mathcal{V}$, and therefore must be incorporated by some other means [21].

The function g in (1) is chosen so that the exact solution reads

$$u\left(\rho,\hat{\theta},\hat{\phi}\right) = h_1^{(2)}\left(kr\left(\rho,\hat{\theta},\hat{\phi}\right)\right) P_1\left(\cos\theta\left(\rho,\hat{\theta},\hat{\phi}\right)\right),$$

where the transformation from prolate spheroidal to spherical coordinates is given by

$$r = \sqrt{\rho^2 - \frac{f^2}{2}\left(1 - \cos 2\hat{\theta}\right)}, \quad \cos\theta = \frac{\rho\cos\hat{\theta}}{\sqrt{\rho^2 - (f^2/2)\left(1 - \cos 2\hat{\theta}\right)}}, \qquad \phi = \hat{\phi}.$$

It has been observed in [32,33] that the UWUC global multipole infinite element formulation yields an approximate solution u_h which gives better accuracy on the boundary $\partial\Omega$ than the approximate solution arising from the conjugated global multipole infinite element formulation. Consequently, we are interested in investigating the behavior on the boundary $\partial\Omega$ of the approximate solution u_h arising from the UWUC piecewise multipole infinite element formulation and comparing this behavior to that of the UWUC global multipole infinite element. In order to observe this behavior on the boundary $\partial\Omega$, we consider the function space $L^2(\partial\Omega)$ endowed with the norm given in (14).

Unconjugated Piecewise Multipole Infinite Element

The piecewise multipole infinite element is formulated with the UWUC weak formulation in exactly the same fashion as was done with the WC weak formulation. In the radial coordinate, we use the Lagrange shape functions given in (15) and (18) together with transformations given in (16) and (19) and Jacobians given in (17) and (20). In the angular coordinates, we introduce Lagrange polynomial shape functions $\chi_i(\xi,\eta)$ introduced in (22) where the transformation from local coordinates (ξ,η) to global angular coordinates $(\hat{\theta},\hat{\phi})$ is given in (21). Again, the elemental shape functions $\varphi_j(\rho,\xi,\eta)$ are the tensor product of the radial shape functions with the angular shape functions.

As previously, introducing the approximate solution and test functions

$$u_h(\rho,\xi,\eta) = \sum_{\lambda=1}^{n_n}\sum_{\nu=1}^{m_n} u_{(\lambda-1)m_n+\nu}\sigma_\lambda(\rho)\chi_\nu(\xi,\eta), \qquad v_h(\rho,\xi,\eta) = \sigma_\kappa(\rho)\chi_\mu(\xi,\eta)$$

into the weak form (26)–(28) yields the following system of linear equations:

$$\sum_{\lambda=1}^{n_n}\sum_{\nu=1}^{m_n}\left(R_1^{\kappa\lambda}A_3^{\mu\nu} + R_2^{\kappa\lambda}A_2^{\mu\nu} + R_3^{\kappa\lambda}A_1^{\mu\nu}\right) u_{(\lambda-1)m_n+\nu} = V^\kappa W^\mu, \tag{29}$$

for $\kappa = 1,2,\ldots,n_n$ and $\mu = 1,2,\ldots,m_n$. Here $R_1^{\kappa\lambda}$, $R_2^{\kappa\lambda}$, $R_3^{\kappa\lambda}$, V^κ are matrices involving only radial integrations, and $A_1^{\mu\nu}$, $A_1^{\mu\nu}$, $A_1^{\mu\nu}$, W^μ are matrices involving only angular integrations.

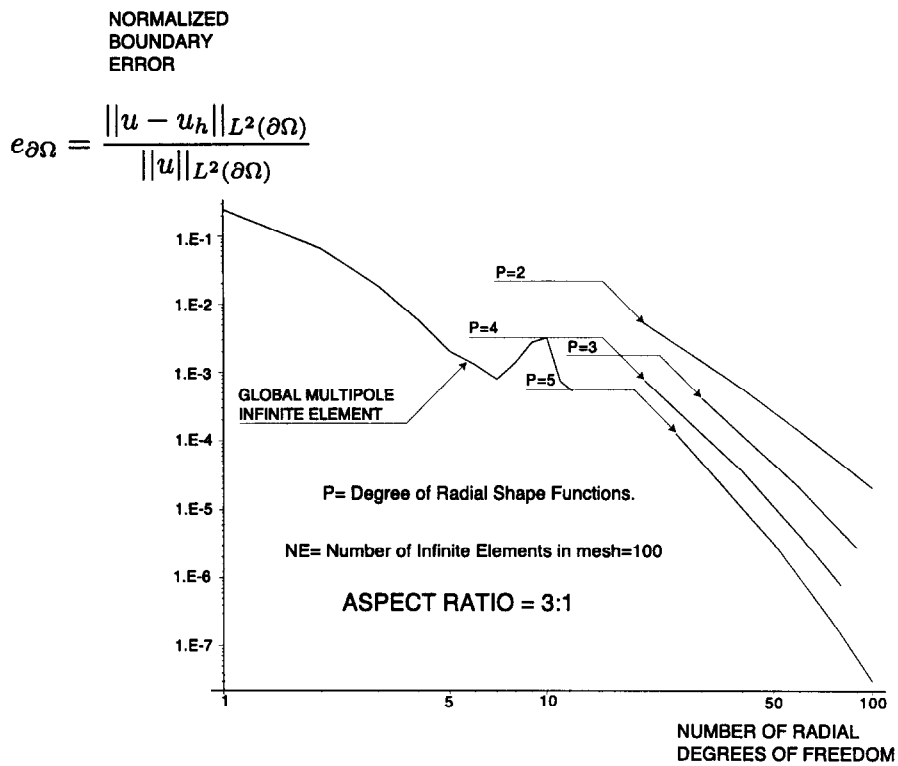

Figure 11. Comparison of the boundary convergence curves of the global multipole and piecewise multipole infinite elements. Unweighted and unconjugated formulation. Aspect ratio = 3:1. Uniform radial mesh.

Only one of these radial Gram matrices which we will take to be $R_1^{\kappa\lambda}$ involves oscillatory terms which are undefined in the limit $\rho \to \infty$; however, these undefined oscillatory terms are canceled out before the limit as $\rho \to \infty$ is taken [16–20].

Convergence Study of the Piecewise Multipole Infinite Element

Using the UWUC weak formulation, a *preconditioned version* of the piecewise multipole infinite element was applied to solve the exterior wave problem (1) with $k = 1$. The preconditioning method applied here to the UWUC piecewise multipole infinite element is very similar to the preconditioning method described in [39], and the preconditioning transformation is constructed to "diagonalize" the radial Gram matrix $R_1^{\kappa\lambda}$ in (29). In this convergence study, we will consider the two prolate spheroidal boundaries $\partial\Omega$ of radius $\rho_1 = 11$ and having aspect ratios of 3:1 and 7:1, respectively. The radial nodes for this infinite element are distributed according to the schemes given in (24) and (25), and the infinite element meshes are illustrated in Figures 3 and 6. The normalized error e_Ω on Ω measured via the norm given in (13) is

$$e_\Omega = \frac{\|u - u_h\|_{H^1_w(\Omega)}}{\|u\|_{H^1_w(\Omega)}},$$

and the normalized boundary error $e_{\partial\Omega}$ on the boundary $\partial\Omega$ measured via the norm given in (14) is

$$e_{\partial\Omega} = \frac{\|u - u_h\|_{L^2(\partial\Omega)}}{\|u\|_{L^2(\partial\Omega)}}.$$

The convergence results given in Figures 11–19 compares the performance of the UWUC piecewise multipole infinite elements with the UWUC global multipole infinite element. Each infinite element utilizes fifth-order Lagrange polynomial shape functions in the angular variable θ, and

NORMALIZED ERROR

$$e_\Omega = \frac{||u - u_h||_{H^1_w(\Omega)}}{||u||_{H^1_w(\Omega)}}$$

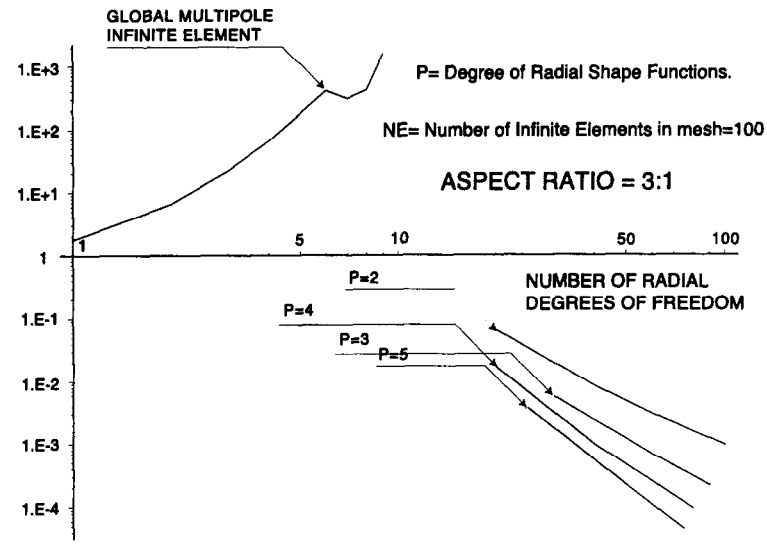

Figure 12. Comparison of the domain convergence curves of the global multipole and piecewise multipole infinite elements. Unweighted and unconjugated formulation. Aspect ratio = 3:1. Uniform radial mesh.

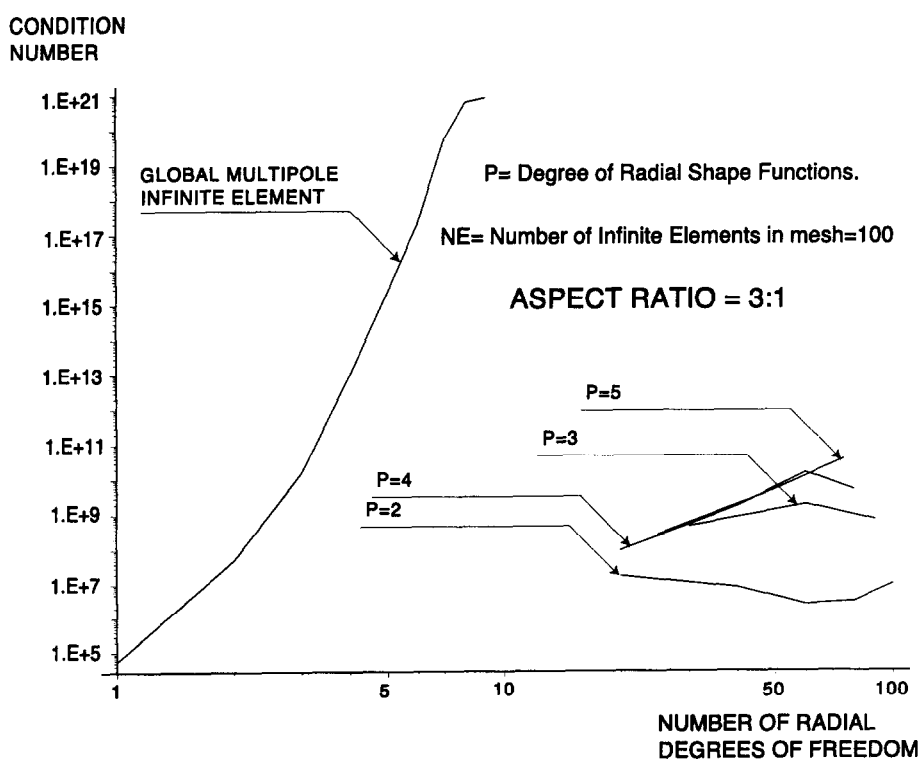

Figure 13. Comparison of the assembled stiffness matrix condition numbers of the global multipole and piecewise multipole infinite elements. Unweighted and unconjugated formulation. Aspect ratio = 3:1. Uniform radial mesh.

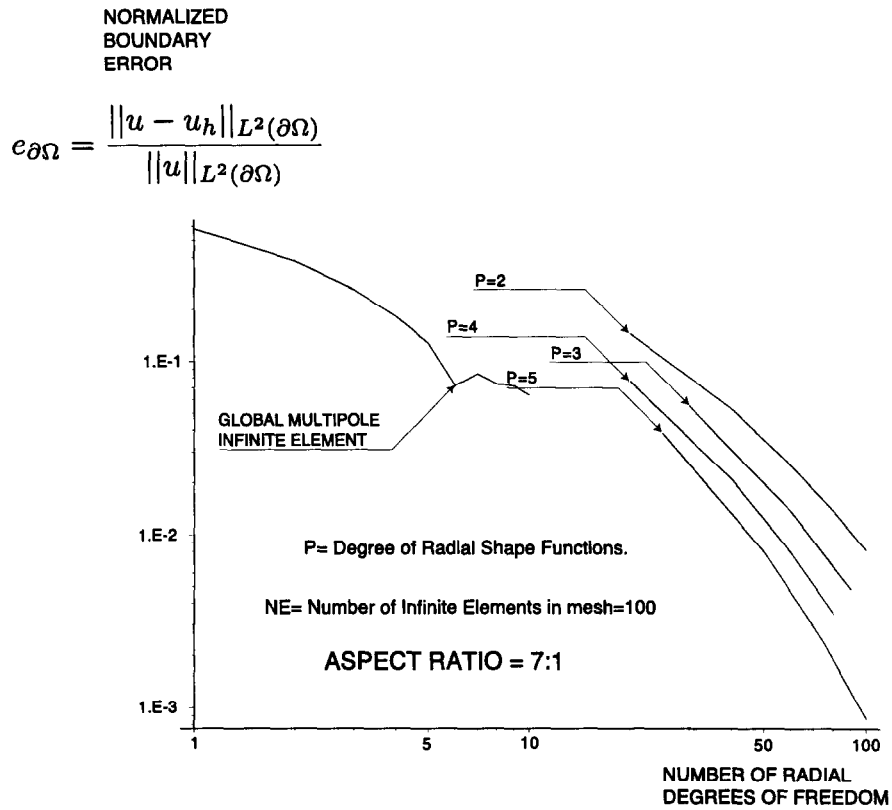

Figure 14. Comparison of the boundary convergence curves of the global multipole and piecewise multipole infinite elements. Unweighted and unconjugated formulation. Aspect ratio = 7:1. Uniform radial mesh.

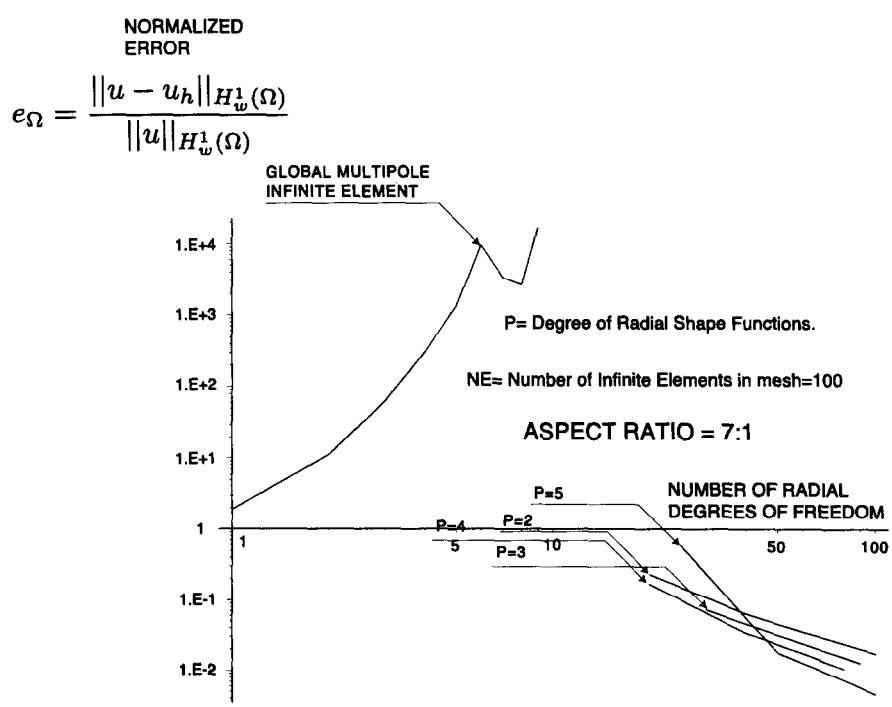

Figure 15. Comparison of the domain convergence curves of the global multipole and piecewise multipole infinite elements. Unweighted and unconjugated formulation. Aspect ratio = 7:1. Uniform radial mesh.

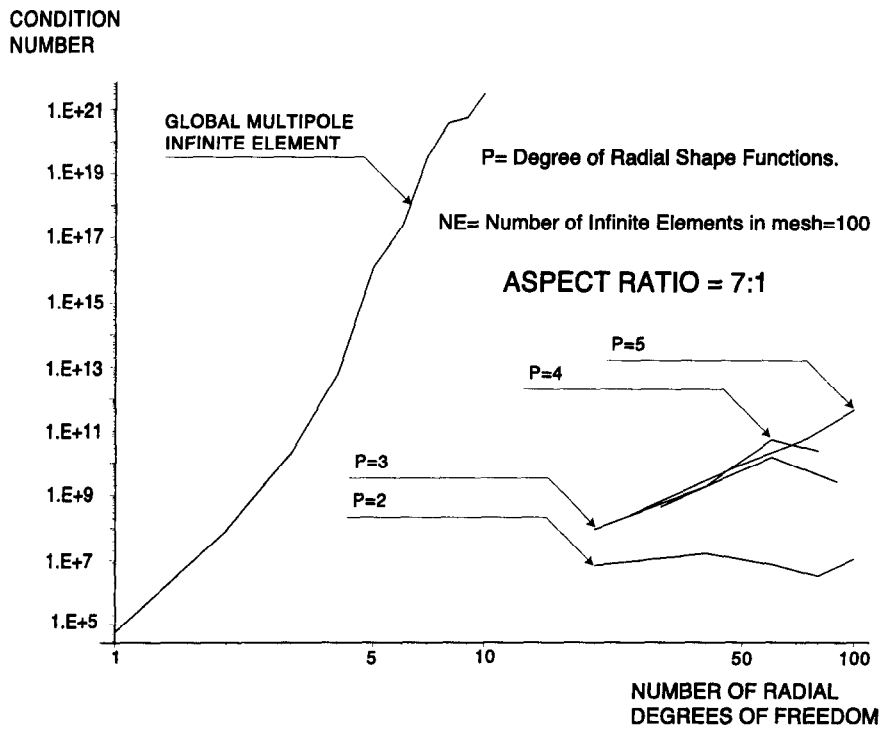

Figure 16. Comparison of the assembled stiffness matrix condition numbers of the global multipole and piecewise multipole infinite elements. Unweighted and unconjugated formulation. Aspect ratio = 7:1. Uniform radial mesh.

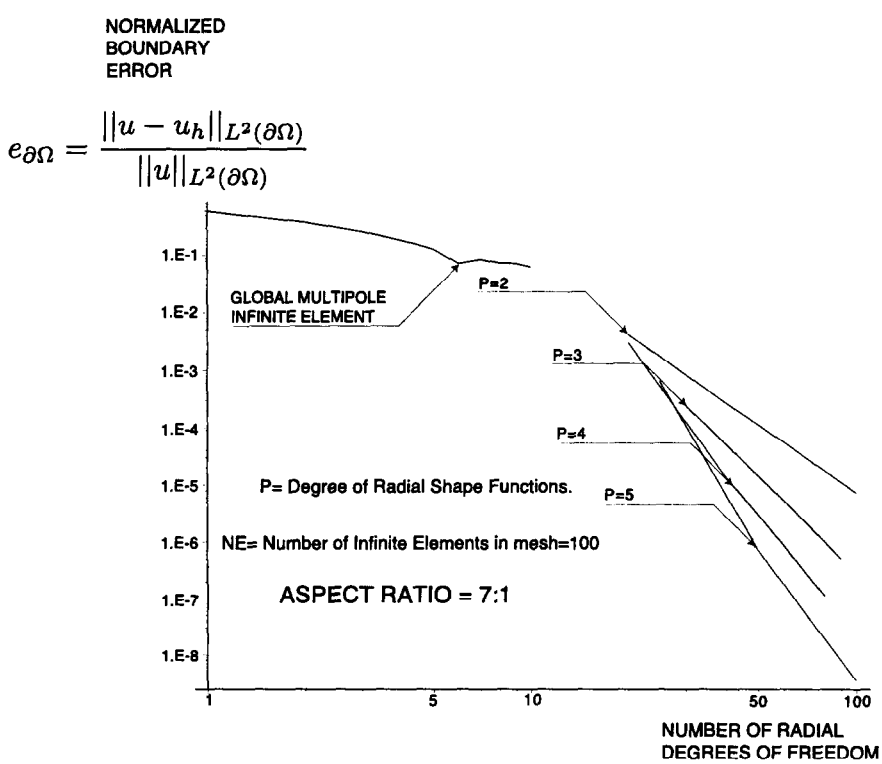

Figure 17. Comparison of the boundary convergence curves of the global multipole and piecewise multipole infinite elements. Unweighted and unconjugated formulation. Aspect ratio = 7:1. Nonuniform radial mesh.

NORMALIZED ERROR

$$e_\Omega = \frac{||u - u_h||_{H^1_w(\Omega)}}{||u||_{H^1_w(\Omega)}}$$

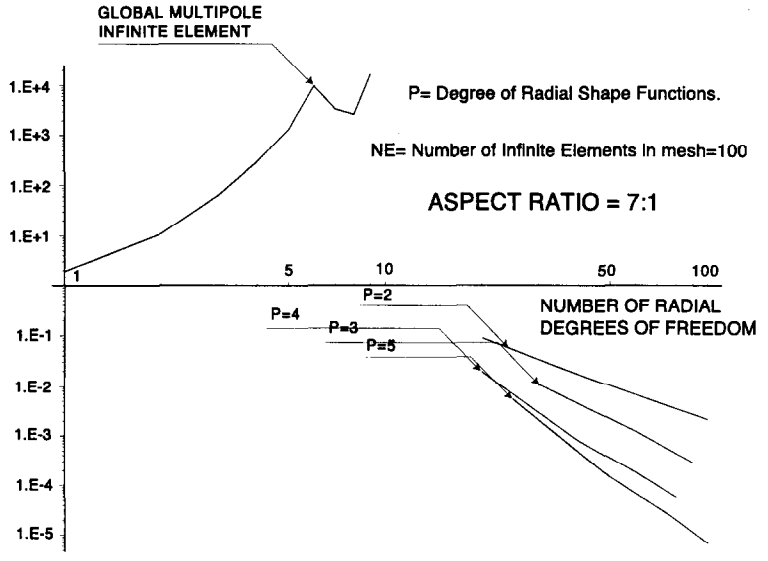

Figure 18. Comparison of the domain convergence curves of the global multipole and piecewise multipole infinite elements. Unweighted and unconjugated formulation. Aspect ratio = 7:1. Nonuniform radial mesh.

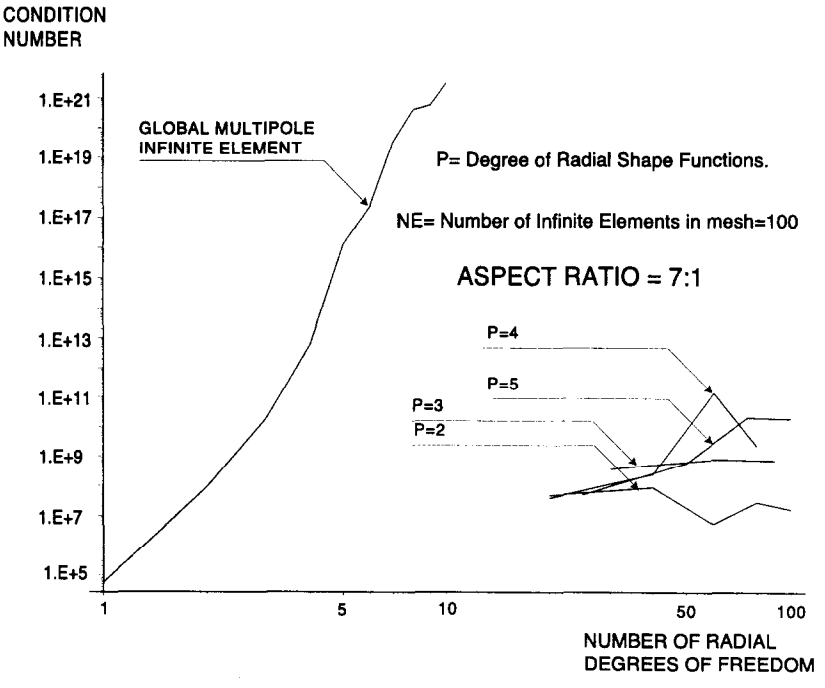

Figure 19. Comparison of the assembled stiffness matrix condition numbers of the global multipole and piecewise multipole infinite elements. Unweighted and unconjugated formulation. Aspect ratio = 7:1. Nonuniform radial mesh.

each piecewise infinite element utilizes p^{th}-order Lagrange polynomial shape functions in the variable $1/\rho$. The infinite element meshes considered in this convergence study consist of 100 infinite elements. All computations in this convergence study were done using standard 16-digit precision arithmetics.

Figures 11, 14, and 17 show the normalized boundary error $e_{\partial\Omega}$ graphed against the number of radial degrees of freedom in logarithmic coordinates for the aspect ratios of 3:1 and 7:1, respectively. It is observed that the global multipole element gives an exponential rate of convergence on the boundary until the number of multipole terms reaches 5. When the number of multipole terms exceeds 5, a divergent behavior begins to occur apparently due to ill-conditioning. Each p^{th}-order piecewise multipole element also gives convergence, and each convergence curve appears to be linear. For the 3:1 aspect ratio, the minimum boundary error achieved by the global multipole element is $e_{\partial\Omega} \approx 5 \times 10^{-4}$, while the minimum boundary error achieved by the piecewise multipole elements is $e_{\partial\Omega} \approx 3 \times 10^{-8}$ with the uniform radial mesh. For the 7:1 aspect ratio, the minimum boundary error achieved by the global multipole element is $e_{\partial\Omega} \approx 5 \times 10^{-2}$. The minimum boundary error achieved by the piecewise multipole elements is $e_{\partial\Omega} \approx 1 \times 10^{-3}$ with the uniform radial mesh and $e_{\partial\Omega} \approx 1 \times 10^{-8}$ with the nonuniform radial mesh.

Figures 12, 15, and 18 show the normalized error e_Ω graphed against the number of radial degrees of freedom in logarithmic coordinates for the aspect ratios of 3:1 and 7:1, respectively. It is observed that each piecewise multipole infinite element gives convergence in the radial direction, and each convergence curves appears to be linear. However, the global multipole infinite element exhibits a divergent behavior on the domain Ω which is consistent with the findings of Shirron and Babuška [32,33]. The minimum error achieved by the piecewise multipole element for the 3:1 aspect ratio is $e_\Omega \approx 5 \times 10^{-5}$, and for the 7:1 aspect ratio the minimum error achieved is $e_\Omega \approx 5 \times 10^{-3}$ with the uniform radial mesh and $e_\Omega \approx 7 \times 10^{-6}$ with the nonuniform radial mesh.

Figures 13, 16, and 19 show the stiffness matrix condition numbers graphed against the number of radial degrees of freedom in logarithmic coordinates. The condition number of the global multipole element grows exponentially while it appears that the condition number of each p^{th}-order piecewise multipole infinite element grows linearly. Moreover, the levels of ill-conditioning for the piecewise multipole elements are more acceptable than that of the global multipole element. Comparing Figures 13, 16, and 19 with Figures 5, 8, and 10, we see that the levels of ill-conditioning of the preconditioned UWUC piecewise multipole infinite elements are somewhat higher than those of the WC piecewise multipole infinite elements. This may be due to the fact that the UWUC bilinear form (27) is unstable, whereas the WC sesquilinear form (11) is stable [32,33].

5. CONCLUSIONS AND SUGGESTIONS FOR FURTHER RESEARCH

1. From the results presented in Sections 3 and 4, it is seen that the piecewise infinite elements based on the spheroidal multipole expansion (9) appear to converge on the domain Ω and on the boundary $\partial\Omega$ when implemented with either the WC or UWUC weak formulations. The global multipole infinite element, utilizing radial functions with global support, has limited approximation accuracy due to numerical ill-conditioning and does not give convergence on Ω when implemented with the UWUC weak formulation. However, by replacing the radial functions which have global support with radial functions which have local support, the numerical ill-conditioning seems to be remedied very well. The resulting piecewise multipole infinite element appears to have good numerical conditioning and convergence properties when implemented with either the WC or UWUC weak formulations and seems to have improved performance as compared to the global multipole infinite element. Another advantage of the piecewise multipole infinite element is that the radial

degrees of freedom may be distributed optimally by means of node relocation. This may result in a significant decrease of the approximation error.

2. The level of numerical ill-conditioning of a preconditioned version of the UWUC piecewise multipole infinite element is still somewhat higher than the WC piecewise multipole infinite element. A possible method to further decrease the level of numerical ill-conditioning of the UWUC piecewise element might be to apply a preconditioning method which is an extension to multiple radial operators of the preconditioning method described in [39]. In this extended method, a preconditioning transformation would be constructed to "diagonalize" all three radial Gram matrices $R_1^{\kappa\lambda}$, $R_2^{\kappa\lambda}$, $R_3^{\kappa\lambda}$ in (29) instead of just the single radial Gram matrix $R_1^{\kappa\lambda}$ in (29) as was done in this paper. More research is needed to determine if this idea will further decrease the level of numerical ill-conditioning of the UWUC piecewise multipole infinite element.

REFERENCES

1. P. Bettess, Infinite elements, *International Journal for Numerical Methods in Engineering* **11**, 53–64, (1977).
2. P. Bettess and O.C. Zienkiewicz, Diffraction and refraction of surface waves using finite and infinite elements, *International Journal for Numerical Methods in Engineering* **11**, 1271–1290, (1977).
3. P. Bettess, More on infinite elements, *International Journal for Numerical Methods in Engineering* **15**, 1613–1626, (1980).
4. O.C. Zienkiewicz, C. Emson and P. Bettess, A novel boundary infinite element, *International Journal for Numerical Methods in Engineering* **19**, 393–404, (1983).
5. O.C. Zienkiewicz, K. Bando, P. Bettess, C. Emson and T.C. Chiam, Mapped infinite elements for exterior wave problems, *International Journal for Numerical Methods in Engineering* **21**, 1229–1251, (1985).
6. P. Bettess and J.A. Bettess, Infinite elements for dynamic problems: Part 1, *Engineering Computations* **8**, 99–124, (1991).
7. P. Bettess and J.A. Bettess, Infinite elements for dynamic problems: Part 2, *Engineering Computations* **8**, 125–151, (1991).
8. P. Bettess and E. Chadwick, Wave envelope examples for progressive waves, *International Journal for Numerical Methods in Engineering* **38**, 2487–2508, (1995).
9. J.A. Bettess and P. Bettess, A new mapped infinite wave element for general wave diffraction problems and its validation on the ellipse diffraction problem, *Exterior Problems of Wave Propagation,* Special Issue of *Computer Methods in Applied Mechanics and Engineering,* (Edited by D. Givoli and I. Harari) **164**, 17–48, (1998).
10. J.A. Bettess and P. Bettess, New mapped wave infinite element and diffraction of waves by elliptical cylinders of varying aspect ratio, In *Fluid Mechanics and Its Applications, Volume 49,* (Series Editor R. Moreau), Proceedings of the IUTAM Symposium on Computational Methods for Unbounded Domains, Boulder, CO, July 27–31, 1997, (Edited by T.L. Geers), pp. 33–42, Kluwer Academic, Norwell, MA, (1998).
11. R.J. Astley, G.J. Macaulay and J.P. Coyette, Mapped wave envelope elements for acoustical radiation and scattering, *Journal of Sound and Vibration* **170**, 97–118, (1994).
12. L. Cremers, K.R. Fyfe and J.P. Coyette, A variable order infinite acoustic wave envelope element, *Journal of Sound and Vibration* **171**, 483–508, (1994).
13. R.J. Astley, Mapped spheroidal wave-envelope elements for unbounded wave problems, *International Journal for Numerical Methods in Engineering* **41**, 1235–1254, (1998).
14. R.J. Astley, Transient spheroidal elements for unbounded wave problems, *Exterior Problems of Wave Propagation,* Special Issue of *Computer Methods in Applied Mechanics and Engineering,* (Edited by D. Givoli and I. Harari) **164**, 3–15, (1998).
15. R.J. Astley, Recent advances in applying wave-envelope elements to unbounded wave problems, In *Fluid Mechanics and Its Applications, Volume 49,* (Series Editor R. Moreau), Proceedings of the IUTAM Symposium on Computational Methods for Unbounded Domains, Boulder, CO, July 27–31, 1997, (Edited by T.L. Geers), pp. 11–20, Kluwer Academic, Norwell, MA, (1998).
16. D.S. Burnett, A three-dimensional acoustic infinite element based on a prolate spheroidal multipole expansion, *Journal of the Acoustical Society of America* **96**, 2798–2816, (1994).
17. D.S. Burnett, Erratum: A three-dimensional acoustic infinite element based on a prolate spheroidal multipole expansion [*Journal of the Acoustical Society of America* **96**, 2798–2816, (1994)], *Journal of the Acoustical Society of America* **97**, 2607, (1995).
18. D.S. Burnett and R.L. Holford, Prolate and oblate spheroidal acoustic infinite elements, *Computer Methods in Applied Mechanics and Engineering* **158**, 117–141, (1998).
19. D.S. Burnett and R.L. Holford, An ellipsoidal acoustic infinite element, *Exterior Problems of Wave Propagation,* Special Issue of *Computer Methods in Applied Mechanics and Engineering,* (Edited by D. Givoli and I. Harari) **164**, 49–76, (1998).

20. D.S. Burnett and R.L. Holford, Multipole-based 3-D infinite elements: An ellipsoidal acoustic element and a spherical electromagnetic element, In *Fluid Mechanics and Its Applications, Volume 49*, (Series Editor R. Moreau), Proceedings of the IUTAM Symposium on Computational Methods for Unbounded Domains, Boulder, CO, July 27–31, 1997, (Edited by T.L. Geers), pp. 53–62, Kluwer Academic, Norwell, MA, (1998).
21. L. Demkowicz and K. Gerdes, Convergence of the infinite element methods for the Helmholtz equation in separable domains, *Numerische Mathematik* **79**, 11–42, (1998).
22. K. Gerdes and L. Demkowicz, Solution of 3D-Laplace and Helmholtz equations in exterior domains using hp-infinite elements, *Computer Methods in Applied Mechanics and Engineering* **137**, 239–273, (1996).
23. W. Cecot, L. Demkowicz and W. Rachowicz, A two-dimensional infinite element for Maxwell's equations, TICAM Report, The University of Texas at Austin, TX, 1–36, (1998).
24. L. Demkowicz and M. Pal, An infinite element for Maxwell's equations, *Exterior Problems of Wave Propagation,* Special Issue of *Computer Methods in Applied Mechanics and Engineering,* (Edited by D. Givoli and I. Harari) **164**, 77–94, (1998).
25. L. Demkowicz and F. Ihlenburg, Proof of convergence for the coupled finite/infinite element methods for Helmholtz exterior boundary-value problems, In *Fluid Mechanics and Its Applications, Volume 49*, (Series Editor R. Moreau), Proceedings of the IUTAM Symposium on Computational Methods for Unbounded Domains, Boulder, CO, July 27–31, 1997, (Edited by T.L. Geers), pp. 83–93, Kluwer Academic, Norwell, MA, (1998).
26. L. Demkowicz and F. Ihlenburg, Analysis of a coupled finite-infinite element method for exterior Helmholtz problems, TICAM Report, The University of Texas at Austin, TX, 1–29, (1998).
27. K. Gerdes, A summary of infinite element formulations for exterior Helmholtz problems, *Exterior Problems of Wave Propagation,* Special Issue of *Computer Methods in Applied Mechanics and Engineering,* (Edited by D. Givoli and I. Harari) **164**, 95–105, (1998).
28. K. Gerdes, Infinite element methods, In *Fluid Mechanics and Its Applications, Volume 49*, (Series Editor R. Moreau), Proceedings of the IUTAM Symposium on Computational Methods for Unbounded Domains, Boulder, CO, July 27–31, 1997, (Edited by T.L. Geers), pp. 143–150, Kluwer Academic, Norwell, MA, (1998).
29. J.L. Cipolla and M.J. Butler, Infinite elements in the time domain using a prolate spheroidal multipole expansion, *International Journal for Numerical Methods in Engineering* **43**, 889–908, (1998).
30. I. Harari, R. Shalom and P. Barbone, Higher-order boundary infinite elements, *Exterior Problems of Wave Propagation,* Special Issue of *Computer Methods in Applied Mechanics and Engineering,* (Edited by D. Givoli and I. Harari) **164**, 107–119, (1998).
31. I. Harari, P.E. Barbone and J.M. Montgomery, Finite element formulations for exterior problems: Application to hybrid methods, non-reflecting boundary conditions, and infinite elements, *International Journal for Numerical Methods in Engineering* **40**, 2791–2805, (1997).
32. J.J. Shirron and I. Babuška, A comparison of approximate boundary conditions and infinite element methods for exterior Helmholtz problems, *Exterior Problems of Wave Propagation,* Special Issue of *Computer Methods in Applied Mechanics and Engineering,* (Edited by D. Givoli and I. Harari) **164**, 121–139, (1998).
33. J.J. Shirron, Solution of exterior Helmholtz problems using finite and infinite elements, Ph.D. Thesis, Department of Applied Mathematics, University of Maryland, (1995).
34. R.L. Holford, A multipole expansion for the acoustic field exterior to a prolate or oblate spheroid, (in preparation).
35. F.V. Atkinson, On Sommerfeld's "radiation condition", *Philosophical Magazine* **40**, 645–651, (1949).
36. C.H. Wilcox, A generalization of theorems of Rellich and Atkinson, *Proceedings of the American Mathematical Society* **7**, 271–276, (1956).
37. C.H. Wilcox, An expansion theorem for electromagnetic fields, *Communications on Pure and Applied Mathematics* **9**, 115–134, (1956).
38. G. Arfken, *Mathematical Methods for Physicists*, Third Edition, Academic Press, San Diego, CA, (1985).
39. A. Safjan and M. Newman, The ill-conditioning of infinite element stiffness matrices, *Computers Math. Applic.* **41** (10/11), 1263–1291, (2001).
40. R.W. Freund, M. Malhorta and P.M. Pinsky, Iterative solution of multiple radiation and scattering problems in structural acoustics using a block quasi-minimal residual algorithm, *Computer Methods in Applied Mechanics and Engineering* **146**, 173–196, (1997).
41. R.D. Cook, *Concepts and Applications of Finite Element Analysis*, Second Edition, John Wiley & Sons, New York, (1981).
42. P.M. Morse, *Vibration and Sound*, The American Institute of Physics for the Acoustical Society of America, (1976).
43. O.C. Zienkiewicz, *The Finite Element Method*, Third Edition, McGraw-Hill, New York, (1977).